Far-field imaging of non-fluorescent species with subdiffraction resolution

Pu Wang[1†], Mikhail N. Slipchenko[1†], James Mitchell[2], Chen Yang[3], Eric O. Potma[4], Xianfan Xu[2] and Ji-Xin Cheng[1,3]*

Super-resolution optical microscopy is providing a new means by which to view as yet unseen details on a nanoscopic scale. Current far-field super-resolution techniques rely on fluorescence as the readout[1–5]. Here, we demonstrate a scheme for breaking the diffraction limit in far-field imaging of non-fluorescent species by using spatially controlled saturation of electronic absorption. Our method is based on a pump–probe process where a modulated pump field perturbs the charge carrier density in a sample, thus modulating the transmission of a probe field. A doughnut-shaped laser beam is then added to transiently saturate the electronic transition in the periphery of the focal volume, so the induced modulation in the sequential probe pulse only occurs at the focal centre. By raster-scanning the three collinearly aligned beams, high-speed subdiffraction-limited imaging of graphite nanoplatelets is performed. This technique has the potential to enable super-resolution imaging of nanomaterials and non-fluorescent chromophores, which may remain out of reach to fluorescence-based methods.

The recently developed pump–probe microscopy technique has allowed label-free imaging of melanin[6,7], chromoproteins and chromogenic reporters[8], epitaxial graphene[9] and carbon nanotubes[10] by perturbing the sample of interest with a modulated pump field and detecting the subsequent material response with an interrogating probe field. Contrast mechanisms in pump–probe microscopy are based on transient absorption processes, including stimulated emission[8,10], ground-state bleaching[11] and excited-state absorption[6]. The existence of a nonlinear optical response in the sample offers the opportunity to break the diffraction limit[2,12]. The method we describe here, which we term 'saturated transient absorption', is related to a group of super-resolution techniques generalized under the concept of reversible saturable optical fluorescence transitions (RESOLFT), in which resolution enhancement is achieved by spatially tailoring the fluorescence emission volume to a sub-diffraction-limited size[1–3,13]. Here, we show the first experimental implementation of this concept for super-resolution imaging of non-fluorescent species using a pump–probe technique. In particular, we demonstrate a diffraction-limit-breaking scheme by ground-state depletion of the charge carrier in graphene-like structures.

Considering a two-state system (shown in the left panel of Fig. 1a), probe photons at ω_{pr} are absorbed to excite the system from L_0 to L_1, leading to a transmission decrease. When a pump field at ω_p is introduced, the pump excitation depletes the population of L_0, thus decreasing the absorption of the probe light accordingly (Fig. 1a, middle panel). When the intensity of the pump field is high enough, it saturates the electronic transition, either by depleting the population at L_0 or by filling the L_1 energy

states. As a result, the transient absorption of probe photons is suppressed (Fig. 1a, right panel). Based on this concept, saturated transient absorption microscopy is designed to decrease the probe area to below the diffraction limit in a pump–probe microscope by collinearly adding a non-modulated saturation beam (ω_{sat}), which has the same wavelength as the pump beam but with much higher intensity (Fig. 1b). At the doughnut-shaped region of the focus where the intensity of the saturation beam is high, the transmission of the probe beam remains unchanged due to saturation of the electronic transition. Under such conditions, the pump-to-probe modulation transfer only occurs at the very centre of the focus where the intensity of the saturation beam is close to zero (Fig. 1c). Subdiffraction-limited images can be obtained by raster-scanning the three collinearly aligned beams simultaneously across the sample.

We used graphene-like structures, whose saturable absorption properties have been studied[14–16], to demonstrate the concept of saturated transient absorption microscopy. Epitaxial graphene has been investigated by pump–probe microscopy, where the pump-induced charge carriers fill the states near the edges of conduction and valence bands, thus reducing probe absorption[9]. As the power of the pump increases, saturable absorption of the pump or absorption bleaching of the probe has been reported as a result of the Pauli blocking process[17]. The relaxation time of the photo-excited charge carriers determines the optimal condition for the pump–probe contrast in graphene-like systems. In brief, the excited carriers first experience a fast carrier–carrier recombination process on a timescale of 20–30 fs (ref. 18), and then interact with optical phonons in a relatively slow process on a timescale ranging from 100 fs to a few picoseconds[19]. As a result, a reasonable contrast from a pump–probe measurement of graphene can be achieved by using pump and probe pulses that have a duration and temporal delay on a subpicosecond scale. To actively suppress the pump–probe signal, an unmodulated, intense saturation pulse is temporally inserted between the pump and probe pulses.

The saturated transient absorption microscope is illustrated in Fig. 2 (for details see Methods). Briefly, a 1,064 nm beam with 260 fs pulse duration was split into pump and saturation beams. An 830 nm beam with 140 fs pulse duration was collinearly aligned with the pump and saturation beams. A spatial light modulator (SLM) was used to engineer the focus of the saturation beam by applying selected phase patterns. All three beams were initially set to be linearly polarized.

Using this set-up, we identified the parameters for effective suppression of the pump–probe signal. We first performed time-resolved pump–probe spectroscopy to characterize the relaxation

[1]Weldon School of Biomedical Engineering, Purdue University, West Lafayette, Indiana 47907, USA, [2]School of Mechanical Engineering and Birck Nanotechnology Center, Purdue University, West Lafayette, Indiana 47907, USA, [3]Department of Chemistry, Purdue University, West Lafayette, Indiana 47907, USA, [4]Department of Chemistry, University of California, Irvine, California 92697, USA; [†]These authors contributed equally to this work.
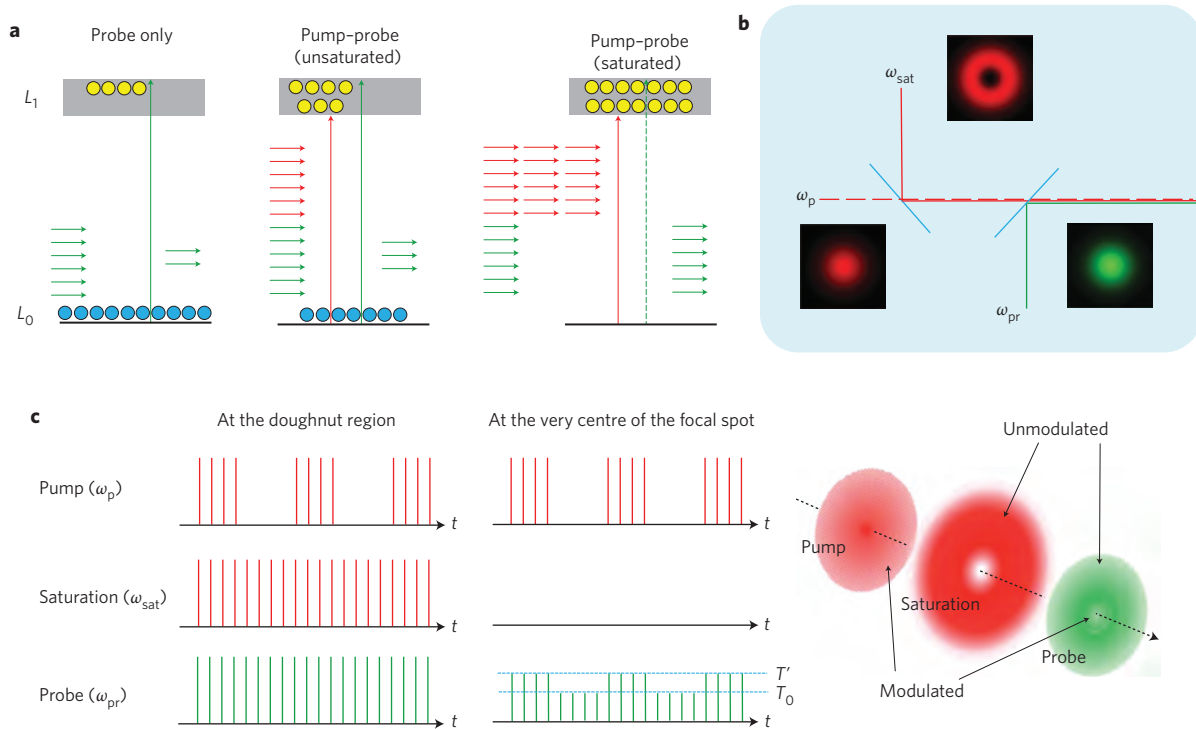*e-mail: jcheng@purdue.edu

Figure 1 | Principle of saturated transient absorption microscopy. a, Illustration of the saturation effect in a two-level electronic transition. Pump and probe photons are indicated by red and green arrows, respectively. **b,** Simple layout of the set-up. The dashed line indicates that the pump beam is modulated. **c,** The pulse train of pump, saturation and probe beams at the focused doughnut-shaped region (left panel) and at the very centre of the focal spot (middle panel). The modulation transfer from pump to probe only occurs at the centre where the saturation field intensity is close to zero (right panel).
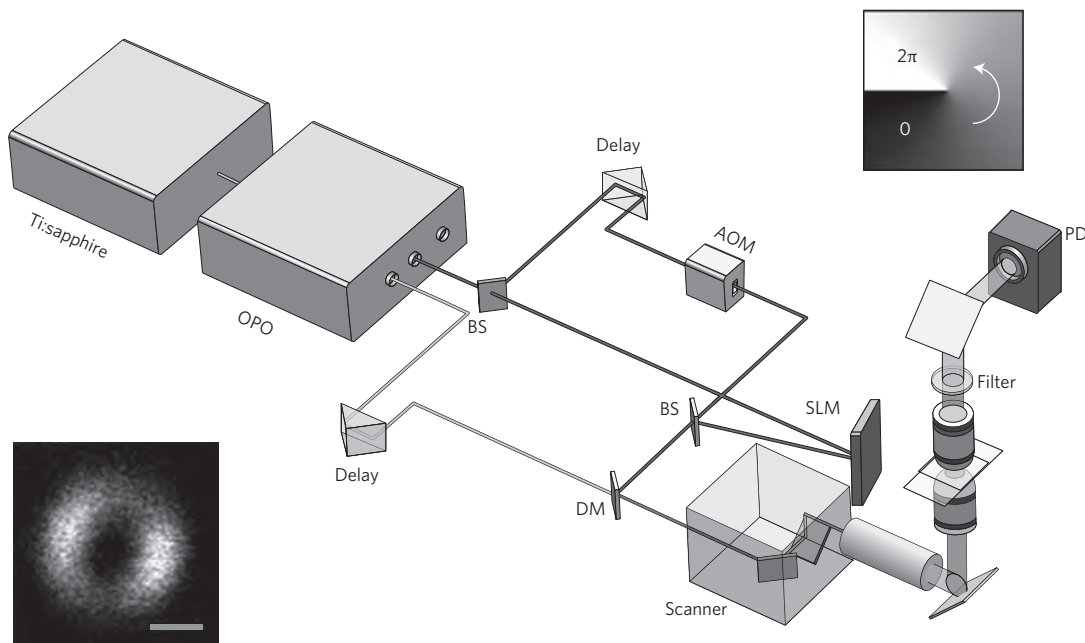
Figure 2 | Diagram of the saturated transient absorption microscope. OPO, optical parametric oscillator; AOM, acousto-optic modulator; BS, beamsplitter; SLM, spatial light modulator; PD, photodiode; DM, dichroic mirror. Upper-right inset: the helix phase pattern sent to the SLM to generate a doughnut-shaped focus of the saturation beam. Lower-left inset: the measured PSF of the saturation beam using second-harmonic imaging of 20 nm ZnO nanocrystals. Scale bar, 500 nm.

time of the photo-excited charge carriers, under the condition such that the powers of the pump and probe beams on the sample were both 0.16 MW cm^{-2}. The transient absorption spectrum of graphene was fitted by a two-component exponential decay model with time constants of 0.4 and 2.0 ps and relative amplitudes of 1.6 and 1.0, respectively (black symbols in Fig. 3a). Because the fast carrier–carrier recombination process (sub-100 fs timescale) cannot be resolved by our system, the fast decay constant represents
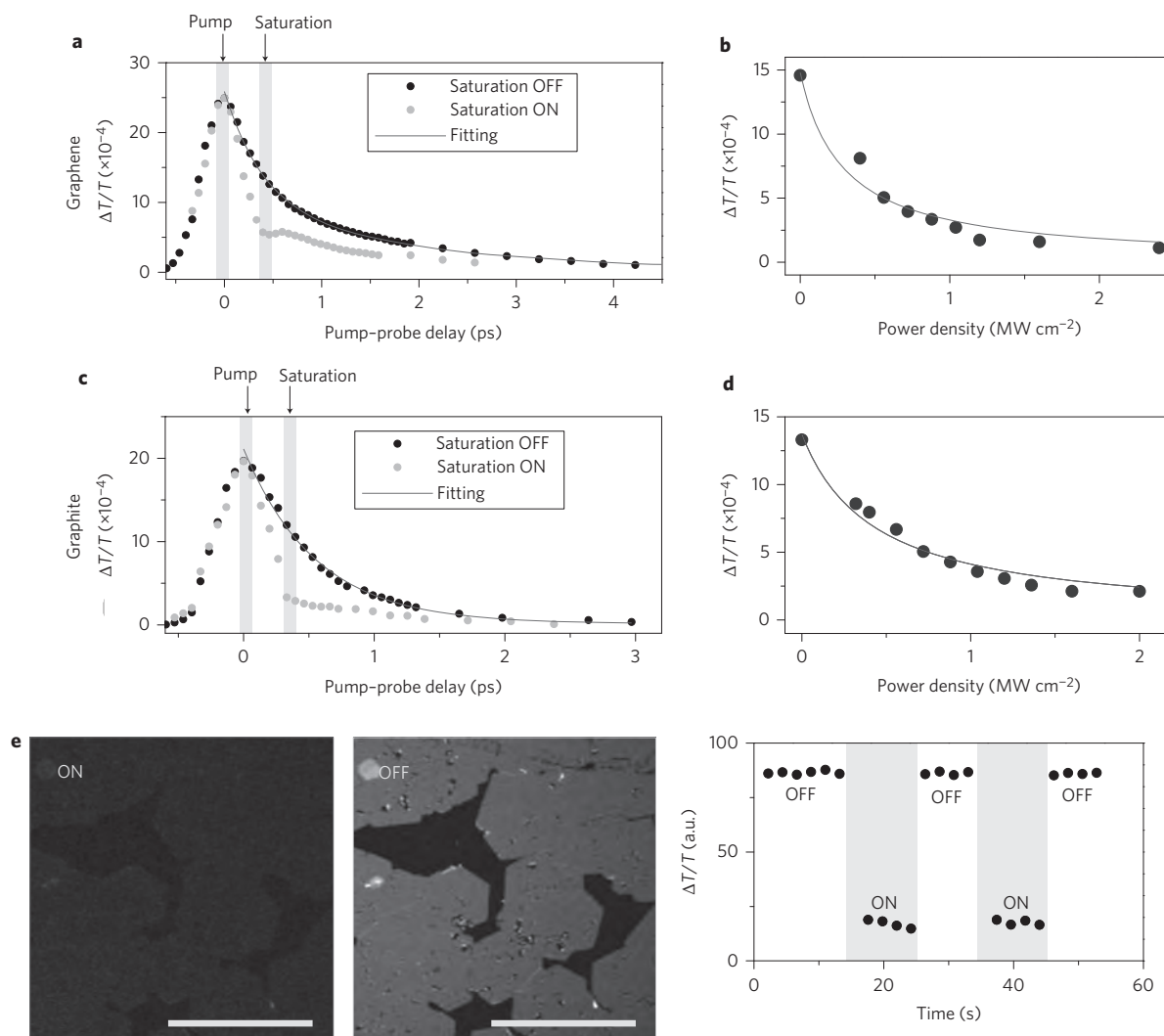
Figure 3 | Suppression of the pump–probe signal by saturation of the electronic transition in graphene and graphite nanoplatelets. a, Time-resolved transient absorption spectroscopy on graphene sample with (grey circles) and without (black circles) saturation beam. **b,** Pump–probe signal as a function of peak power density of the saturation beam on graphene. The fit generates a saturation constant at 0.28 MW cm^{-2}. **c,d,** The same measurements as in **a** and **b**, but for graphite nanoplatelets. **e,** Transient absorption image of graphene with the saturation beam switched on (left) and off (middle). The average intensity for graphene is plotted as a function of time (right). Scale bars, 20 μm.

the instrument response time in these measurements. The slow decay process is attributed to carrier–phonon interaction. We then introduced a saturation pulse with a Gaussian mode and power density of 0.8 MW cm^{-2}. The delay between the pump and saturation pulses was set to ~0.4 ps to avoid interference (Fig. 3a). The pump–probe signal remained unaffected in the first 100 fs, and was quenched significantly after 0.4 ps when the saturation pulse was introduced. The pump–probe signal from graphene as a function of the power density of the saturation beam is plotted in Fig. 3b. The data were fitted by Supplementary equation (S4) and the value of I_0, the power density for saturated absorption, was obtained as 0.28 MW cm^{-2}. The same experiments were performed on graphite nanoplatelets, and characteristics similar to those for graphene were found (Fig. 3c,d). The time constant of the carrier–phonon interaction on graphite nanoplatelets was found to be ~0.6 ps, and I_0 was 0.43 MW cm^{-2}. The recovery of the pump–probe signal was also tested using the graphene sample. As shown in the right panel of Fig. 3e, the signal recovered to nearly 100% when the saturation beam was switched off. No signal degradation was observed during the imaging period of 60 s, under the condition that the power density of the saturation beam was 1.2 MW cm^{-2}

and the dwell time was ~2 s for an image of 512 × 512 pixels. The photodamage began to appear at ~2.4 MW cm^{-2} for the graphite nanoplatelets sample if we repeatedly imaged the same area for 60 s. We therefore applied a saturation beam power lower than the damage threshold for the resolution enhancement experiments.

With these parameters, we conducted label-free far-field imaging of graphite nanoplatelets by applying the doughnut-shaped saturation beam. Conventional pump–probe imaging and saturated transient absorption imaging were performed in the same region (Fig. 4a,b) and visualized by atomic force microscopy (AFM) (Fig. 4c). The power for the saturation beam was set at 2.0 MW cm^{-2}. The intensity shown in the pump–probe images is proportional to the difference transmission of the probe beam, ΔT_{pr}, between pump field on and off states. The nanoplatelets indicated in the AFM images (white arrows in Fig. 4c) could not be resolved in the conventional pump–probe image (Fig. 4a), but were successfully resolved by saturated transient absorption microscopy (Fig. 4b). To quantify the resolution enhancement, we imaged an area where isolated nanoplatelets can be found (Fig. 4d,e). The averaged full-width at half-maximum (FWHM)
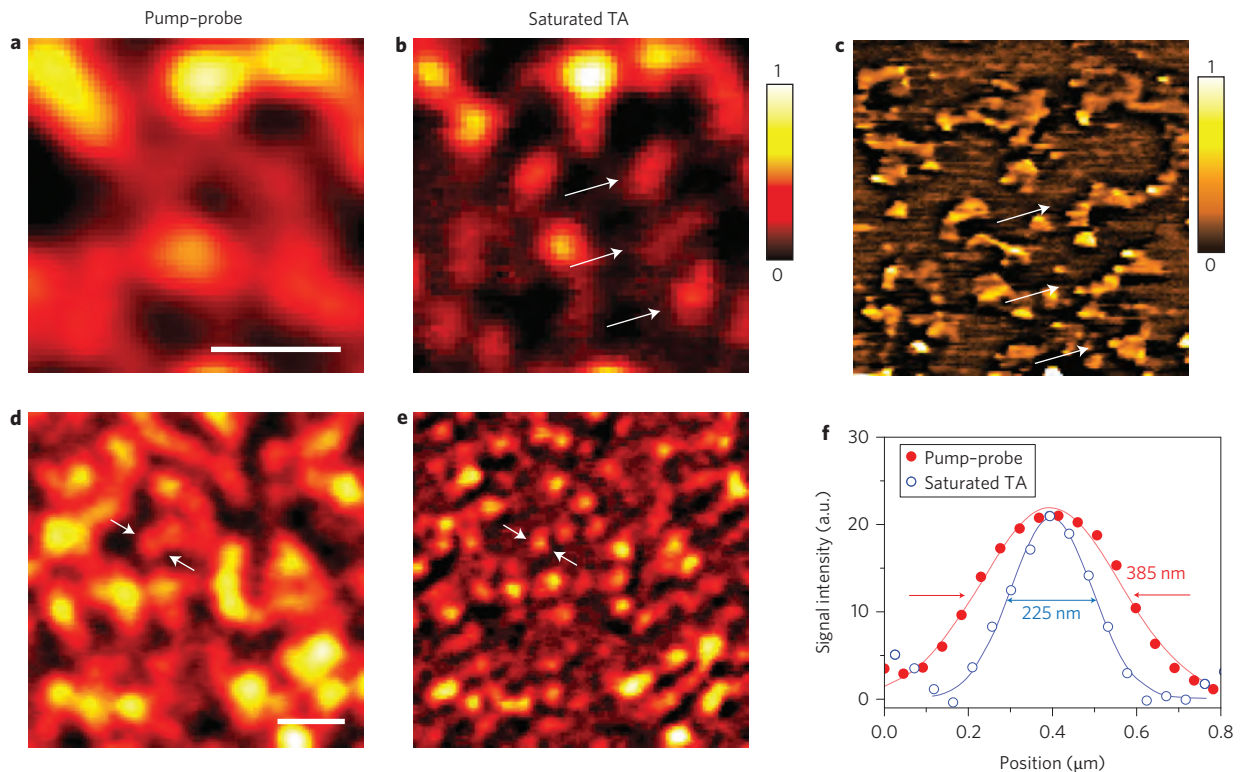
Figure 4 | Subdiffraction-limited imaging of graphite nanoplatelets. a,d, Images obtained by conventional pump–probe microscopy. **b,e,** Images of the same areas obtained by saturated transient absorption microscopy. **c,** AFM images of the graphite nanoplatelets. **f,** Intensity profiles along the lines indicated by the arrows in **d** and **e**. Solid curves represent Gaussian fitting. For comparison of resolution, the peak intensities were normalized to the same value. TA, transient absorption. Scale bars, 1 μm (scale bar in **a** applies to **b** and **c**; scale bar in **d** applies to **e**).

measured in the selected platelets is 249 ± 31 nm (Supplementary Fig. S1). We selected one of the smallest features in the image to characterize the resolution. The line profiles across the selected nanoplatelet (white arrows) obtained by conventional pump–probe and saturated transient absorption are shown in Fig. 4f. By Gaussian fitting of the line profiles (Fig. 4f), the FWHM values for the same isolated object in the conventional pump–probe and saturated transient absorption images were found to be 385 nm and 225 nm, respectively. The line profile is theoretically a convolution of the effective pointspread function (PSF) of the system with the object (Supplementary Section S2). Assuming the average size of the nanoplatelets to be ~100 nm, deconvolution of the line profile and object function using the Gaussian approximation resulted in FWHMs of ~370 nm and 200 nm for the effective PSF of conventional pump–probe and saturated transient absorption microscopy, respectively. Given the nonlinear nature of the pump–probe process and the aperture-free detection scheme, the effective PSF of our pump–probe microscope under diffraction-limited conditions is calculated to be 300 nm (Supplementary Section S2). These results collectively demonstrate that subdiffraction-limited imaging is achievable by the saturated transient absorption microscopy technique.

In summary, we have demonstrated far-field subdiffraction-limited imaging of non-fluorescent samples through spatially controlled saturation of the transient absorption signal. The resolution can be improved further by optimization of the imaging conditions, for example by applying a shorter excitation wavelength and increasing the photodamage threshold with a faster scanning speed. We note that saturated transient absorption microscopy is applicable to other nanomaterials with saturable absorption, such as single-walled carbon nanotubes[20–22] or iron oxide and zinc oxide nanoparticles[23,24], which are considered to be biocompatible

imaging agents[25,26]. Compared to previously reported pump–probe nanoscopy, which is based on scanning tunnelling microscopy or near-field scanning optical microscopy[27], our method offers a much faster imaging speed in a contact-free manner. Moreover, the intrinsic optical sectioning capability of saturated transient absorption microscopy enables three-dimensional imaging with a lateral resolution below the diffraction limit. Resolution enhancement in the axial direction is also possible by applying a z-doughnut beam[28]. These advantages open new opportunities for studying nanostructures in biological environments or inside functional materials.

Methods

120 °C. The coated quartz wafer was covered by another piece of quartz wafer, then mounted on a sample stage in a vacuum chamber. Before growing graphite nanoplatelets, the chamber was pumped and purged by high-purity N_2 gas, and maintained at a pressure below 0.1 torr. A continuous-wave (c.w.) Nd:YAG laser with a wavelength of 532 nm was focused on the S-1805 film through the transparent quartz substrate using a lens with a focal length of 150 mm. With this optical set-up, the graphite nanoplatelet sample was produced with a laser power of 2.8 W, irradiated for 3–5 min. The size and coverage of graphene platelets were determined by the growth parameters. Raman spectroscopy was performed to confirm the composition of the sample (Supplementary Fig. S2). AFM (Veeco Dimension 3100) images were taken in tapping mode under ambient conditions.

Synthesis of graphene. Graphene was grown by thermal chemical vapour deposition on a copper foil, at a temperature of 1,000 °C and under 1 atm pressure, with methane as the precursor gas[30]. Raman spectroscopy was performed to confirm the composition of the sample (Supplementary Fig. S3).

References

1. Hell, S. W. & Wichmann, J. Breaking the diffraction resolution limit by stimulated emission: stimulated-emission–depletion fluorescence microscopy. *Opt. Lett.* **19,** 780–782 (1994).
2. Bretschneider, S., Eggeling, C. & Hell, S. W. Breaking the diffraction barrier in fluorescence microscopy by optical shelving. *Phys. Rev. Lett.* **98,** 218103 (2007).
3. Gustafsson, M. G. L. Nonlinear structured-illumination microscopy: wide-field fluorescence imaging with theoretically unlimited resolution. *Proc. Natl Acad. Sci. USA* **102,** 13081–13086 (2005).
4. Rust, M. J., Bates, M. & Zhuang, X. Sub-diffraction-limit imaging by stochastic optical reconstruction microscopy (STORM). *Nat. methods* **3,** 793–796 (2006).
5. Betzig, E. *et al.* Imaging intracellular fluorescent proteins at nanometer resolution. *Science* **313,** 1642–1645 (2006).
6. Fu, D., Ye, T., Matthews, T. E., Yurtsever, G. & Warren, W. S. Two-color, two-photon, and excited-state absorption microscopy. *J. Biomed. Opt.* **12,** 054004–054008 (2007).
7. Matthews, T. E., Piletic, I. R., Selim, M. A., Simpson, M. J. & Warren, W. S. Pump–probe imaging differentiates melanoma from melanocytic nevi. *Sci. Transl. Med.* **3,** 71ra15 (2011).
8. Min, W. *et al.* Imaging chromophores with undetectable fluorescence by stimulated emission microscopy. *Nature* **461,** 1105–1109 (2009).
9. Huang, L. *et al.* Ultrafast transient absorption microscopy studies of carrier dynamics in epitaxial graphene. *Nano Lett.* **10,** 1308–1313 (2010).
10. Jung, Y. *et al.* Fast detection of the metallic state of individual single-walled carbon nanotubes using a transient-absorption optical microscope. *Phys. Rev. Lett.* **105,** 217401 (2010).
11. Chong, S., Min, W. & Xie, X. S. Ground-state depletion microscopy: detection sensitivity of single-molecule optical absorption at room temperature. *J. Phys. Chem. Lett.* **1,** 3316–3322 (2010).
12. Bouwhuis, G. & Spruit, J. H. M. Optical storage read-out of nonlinear disks. *Appl. Opt.* **29,** 3766–3768 (1990).
13. Hell, S. W. Toward fluorescence nanoscopy. *Nat. Biotechnol.* **21,** 1347–1355 (2003).
14. Sun, Z. *et al.* Graphene mode-locked ultrafast laser. *ACS Nano* **4,** 803–810 (2010).
15. Bao, Q. *et al.* Atomic-layer graphene as a saturable absorber for ultrafast pulsed lasers. *Adv. Funct. Mater.* **19,** 3077–3083 (2009).
16. Vasko, F. T. Saturation of interband absorption in graphene. *Phys. Rev. B* **82,** 245422 (2010).
17. Zitter, R. N. Saturated optical absorption through band filling in semiconductors. *Appl. Phys. Lett.* **14,** 73–74 (1969).
18. Breusing, M., Ropers, C. & Elsaesser, T. Ultrafast carrier dynamics in graphite. *Phys. Rev. Lett.* **102,** 086809 (2009).
19. Wang, H. *et al.* Ultrafast relaxation dynamics of hot optical phonons in graphene. *Appl. Phys. Lett.* **96,** 081917 (2010).
20. Rozhin, A. G. *et al.* Anisotropic saturable absorption of single-wall carbon nanotubes aligned in polyvinyl alcohol. *Chem. Phys. Lett.* **405,** 288–293 (2005).
21. Avouris, P., Freitag, M. & Perebeinos, V. Carbon-nanotube photonics and optoelectronics. *Nature Photon.* **2,** 341–350 (2008).
22. Baek, I. H. *et al.* Single-walled carbon nanotube saturable absorber assisted high-power mode-locking of a Ti:sapphire laser. *Opt. Express* **19,** 7833–7838 (2011).
23. Singh, C. P., Bindra, K. S., Bhalerao, G. M. & Oak, S. M. Investigation of optical limiting in iron oxide nanoparticles. *Opt. Express* **16,** 8440–8450 (2008).
24. Irimpan, L., Nampoori, V. P. N. & Radhakrishnan, P. Spectral and nonlinear optical characteristics of ZnO nanocomposites. *Sci. Adv. Mater.* **2,** 117–137 (2010).
25. Jain, T. K., Reddy, M. K., Morales, M. A., Leslie-Pelecky, D. L. & Labhasetwar, V. Biodistribution, clearance, and biocompatibility of iron oxide magnetic nanoparticles in rats. *Mol. Pharmacol.* **5,** 316–327 (2008).
26. Zhou, J., Xu, N. S. & Wang, Z. L. Dissolving behavior and stability of ZnO wires in biofluids: a study on biodegradability and biocompatibility of ZnO nanostructures. *Adv. Mater.* **18,** 2432–2435 (2006).
27. Terada, Y., Yoshida, S., Takeuchi, O. & Shigekawa, H. Real-space imaging of transient carrier dynamics by nanoscale pump-probe microscopy. *Nature Photon.* **4,** 869–874 (2010).
28. Hein, B., Willig, K. I. & Hell, S. W. Stimulated emission depletion (STED) nanoscopy of a fluorescent protein-labeled organelle inside a living cell. *Proc. Natl Acad. Sci. USA* **105,** 14271–14276 (2008).
29. Slipchenko, M. N., Oglesbee, R. A., Zhang, D., Wu, W. & Cheng, J-X. Heterodyne detected nonlinear optical imaging in a lock-in free manner. *J. Biophoton.* **5,** 801–807 (2012).
30. Cao, H. *et al.* Electronic transport in chemical vapor deposited graphene synthesized on Cu: quantum Hall effect and weak localization. *Appl. Phys. Lett.* **96,** 122106 (2010).

Acknowledgements

Author contributions

P.W., M.N.S. and J.-X.C. designed the experiment. P.W. and M.N.S. performed the experiments. P.W. carried out the data analysis. J.M. synthesized the graphite nanoplatelets. E.O.P. provided the spatial light modulator. J.-X.C., C.Y., E.O.P. and X.X. provided overall guidance to the project. All authors discussed the results and contributed to the manuscript.

Additional information

Supplementary information is available in the online version of the paper. Reprints and permissions information is available online at www.nature.com/reprints. Correspondence and requests for materials should be addressed to J.-X.C.

Competing financial interests

The authors declare no competing financial interests.